PNEUMATIC BOOT FOR HELICOPTER ROTOR DEICING

Bernard J. Blaha and Peggy L. Evanich
Lewis Research Center

SUMMARY

Although they have many desirable characteristics, pneumatic deicer boots have received little consideration for application to helicopters. Modern polyurethane pneumatic deicer boots are light in weight, low in power consumption, easy to control, and capable of field repair. The Lewis Research Center, in cooperation with the B. F. Goodrich Company, has tested pneumatic deicer boots for helicopter rotor blades. The tests were conducted in the Lewis 6- by 9-ft Icing Research Tunnel on a stationary section of a UH-1H helicopter main-rotor blade. The boots were effective in removing ice and in reducing aerodynamic drag due to ice. Results of these tests are presented in this paper. Because of these promising results a program was begun at the NASA Ames Research Center to test boots on full-scale, rotating UH-1H rotor blades.

INTRODUCTION

To date, there are no U.S.-manufactured helicopters certified to fly into forecasted icing conditions. None are expected to be certified for at least 2 years. However, much work is in progress to develop both certification criteria (which currently are not defined exclusively for rotorcraft) and deicing systems for rotors (ref. 1). The rotor deicing systems being developed employ the electrothermal concept (ref. 1). The pneumatic boot concept for rotor blade ice protection was analyzed in 1973 by the Lockheed-California Company and rejected (ref. 2). Although the strong advantages of low weight, low power, blade leading-edge protection, and simple controls were pointed out in this study, Lockheed listed several reasons for questioning the pneumatic boot concept. These reasons included materials problems, possible adverse aerodynamic effects, and basic icing questions. Of the reasons listed, the most damaging centered on the materials technology of the day. A primary question was whether the pneumatic boot could withstand the severe dynamic environment of the helicopter rotor blade. A specific concern was that the boots might be damaged or completely torn off by the high centrifugal forces. Furthermore the rain abrasion resistance of neoprene was unacceptable. Also there were possible adverse aerodynamic effects of the inflated tubes on the small-chord, thin airfoils of a rotor. These problems were sufficient to eliminate the boot from further consideration.

As a result of these early studies the B. F. Goodrich Company has further investigated materials and techniques of pneumatic boot manufacture and has conducted limited testing. They claim that a polyurethane elastomeric material, rather than the currently used neoprene, can be compounded to exhibit

425

many superior properties, such as abrasion (rain and sand) resistance (3 to 5 times greater than that of neoprene), field repairability, greater compatibility to ester oils, higher strength and fatigue resistance, and minimal distortion under high centrifugal forces.

A schematic diagram of the pneumatic system applied to a UH-1H helicopter is shown in figure 1 (ref. 1). According to reference 1 this system would approximately 13.6 kg (30 lb) (43 percent of the electrothermal system weight), would apply to existing rotor blades, and would cost much less than the proposed electrothermal system.

In an initial attempt to evaluate the deicing capability and aerodynamic performance of boots for rotor blades, tests were conducted in 1979 in the NASA Lewis 6- by 9-ft Icing Research Tunnel (IRT) on a 1.83-m (6-ft) span, full-scale segment of a stationary UH-1H rotor blade. In these tests three boot geometries were evaluated. These boots comprised both spanwise and chordwise tubes. Since the model blade was stationary during a run, neither the rotating nor vibrating loads of a real rotor were simulated. Also the high rotor tip speeds could not be simulated since the maximum tunnel air speed was 134 m/sec (i.e., $M_0 \sim 0.4$). Angle of attack was varied from 0° to 16° (stall) without ice and from 0° to 10° with ice. The lower air speeds and the absence of rotor dynamic loads in these tests probably made this a conservative test of the boot's effectiveness as a deicer because both dynamic loads and higher air speeds should aid in removing the ice. Some tests were made to roughly simulate the cyclic motion of a rotor blade by icing the model at one angle of attack and deicing the model at another. With the best boot configuration a series of model drag measurements were made with a translating wake-survey probe. The test results are included herein along with a description of a NASA Ames-Lewis program plan to test the pneumatic boot concept with full-scale, rotating UH-1H blades.

SYMBOLS

C_d section drag coefficient, $2 \int \dfrac{V}{V_0} \left(1 - \dfrac{V}{V_0}\right) dz$

c wing chord, 0.533 m (1.75 ft)

D_{med} droplet median volume size, μm

H local stagnation pressure

H_0 free-stream stagnation pressure

LWC liquid water content, g/m^3

M_0 free-stream Mach number

P_0 free-stream static pressure

T_0 free-stream stagnation temperature, $^{\circ}C$

X, Z position coordinates, m

V velocity, m/sec

V_0 free-stream velocity, m/sec

α section angle of attack at tunnel centerline, deg

TEST APPARATUS AND PROCEDURE

The test model was made from a 1.83-m (6-ft) span segment of a full-scale UH-1H rotor blade and was mounted vertically in the test section of the Lewis 6- by 9-ft Icing Research Tunnel (fig. 2). Since the model was cut from an actual rotor blade, it included a uniform twist of approximately 0.5° per foot or about 3° from floor to ceiling. The rotor blade on a UH-1H helicopter is 14.63 m (48 ft) in diameter and incorporates a constant-chord (0.533 m (1.76 ft)) NACA 0012 airfoil section. The model was mounted on the tunnel floor-plate, and the angle of attack could be varied from near zero to stall.

The pneumatic boots were applied over the external surface of the leading edge, and the supply air line was routed inside the model and through the tunnel floorplate. The control system for the boot test was the same as that shown in figure 1. For the wind tunnel tests the turbine bleed air was replaced by regulated tunnel service air. This system is also the same as the one currently used on fixed-wing aircraft. The system was designed around a two-position valve (ejector flow control valve) that used a venturi orifice to provide vacuum to the boot when it was not activated. Upon activation this valve closed and higher pressure air (10.5×10^3 to 21×10^3 kg/m^2 (15 to 30 psig)) was provided to rapidly inflate the boot. This system can be operated either manually or automatically with a programed pulse sequence and timing.

A translating wake-survey probe was used to help evaluate the deicing performance of the boot configurations. The probe, as shown in figure 3, consisted of a single stagnation pressure tube that could be retracted down behind a wind screen. When the airfoil was exposed to the tunnel icing cloud, the probe was retracted behind the windscreen. Then after the cloud was turned off, the probe was inserted into the air stream and the wake survey was made. This probe, which was located about one chord downstream of the airfoil at midspan, was installed as shown in figure 4 to yield the velocity decrement ratio V/V_0 in the airfoil wake. By translating laterally through the wake a plot of V/V_0 as a function of position X was obtained. Integration of the wake defect gave a measurement of airfoil section drag coefficient.

Sketches of the pneumatic boot designs tested are shown in figures 5 and 6. In the initial part of the test program three candidate designs were screened in terms of their deicing capability. These boots were designed to use a combination of both chordwise and spanwise tubes. Results from tests

performed in the 1950's (ref. 3) on pneumatic boots for fixed wings suggested that the aerodynamic effect of inflating the tubes was less with chordwise tubes than with spanwise configurations. Because the rotor airfoil section was both shorter and thinner than fixed wings, it was felt that the boot for a helicopter rotor should incorporate primarily chordwise tubes. However, with the small leading-edge radius of a rotor blade, it was evident that chordwise tubes would crimp over in the leading-edge region and not provide the deflection necessary to fracture and remove the ice. As a result it was necessary to also incorporate into the boot design a spanwise tube (or tubes) at the leading edge. Two boot geometries were tested initially: a small-diameter-tube configuration (similar to fig. 5, but with a single spanwise tube) and a larger-diameter-tube configuration (fig. 6). These boot configurations incorporated tube sizes that were in the same range (1.27 to 3.18 cm diam) as those currently used on larger chord, fixed-wing aircraft. For the smaller-chord rotor airfoils it would be desirable to use smaller diameter tubes to minimize the aerodynamic effect, especially upon accidental or multiple inflation. However, getting the deflections required to break the ice with smaller tubes would require higher inflation pressures than available on existing rotorcraft. Consequently the tube sizes used in this program were from 5 to 7 times larger, relative to the chord length, than those currently used for fixed wings. The boots were designed to provide coverage of about 20 percent of the chord on the upper surface and 30 percent on the lower. When choosing the amount of chordwise boot coverage, both the limits of impingement of water-droplet trajectories and runback should be taken into account.

During the initial deicing tests the two configurations with a single spanwise tube on the leading edge were ineffective in removing the ice. Therefore, as discussed in the section RESULTS AND DISCUSSION, the boot design was modified by splitting the single spanwise tube into two tubes (fig. 5). Once it was determined that the boot with two spanwise tubes on the leading edge was effective in deicing the blade, the translating probe was installed. Measurements of airfoil section drag near the model centerline were made over a range in angle of attack from 0° to stall (~16° without ice, and ~9.4° with ice). Data were obtained, both with and without the boot installed, at tunnel speeds of 67 and 112 m/sec (150 and 250 mph). These speeds are lower than those near the outboard sections of a rotor blade; therefore compressibility effects and aerodynamic heating effects were not simulated. Data were initially taken at the lower speed, without ice, to check out the probe and to check the stall characteristics of the rotor blade. Stall was determined by applying tufts to the suction surface of the blade and observing where the flow began to reverse direction or become unstable. When it was determined that the probe could withstand the turbulence generated by the model, data were taken at the higher speed with ice.

Data were obtained at various icing conditions and at various angles of attack. By selecting tunnel temperature both glaze (-6.1° C) and rime (-14.4° C) ice conditions were investigated. In all cases the icing cloud conditions were kept constant at a volume median droplet size D_{med} of 20 µm and a liquid water content (LWC) of 1 g/m^3. Most icing and deicing sequences were done at constant angles of attack, but for some conditions the model would be iced at one angle of attack and deiced at another. The angles of attack were kept within the range of those typically expected on a rotor blade, namely,

between 0° and 8°. For example the model would be iced at 1.4° and deiced at 5.4°, or vice versa; the model was also iced at 5.4° and deiced at 9.4°. These variations were an attempt to simulate, in a very slow way, the cyclic pitch variations of a real rotor blade.

In each icing test sequence about 1 cm of ice was accreted on the blade before deicing was attempted. One centimeter of ice was chosen as a good test condition for two reasons. First, for the pneumatic boot to work, a certain amount of ice has to be present. If too little ice is present, the ice will be fractured into small pieces, but the interfacial bonds will not be broken and consequently the ice will not be removed. Second, from unpublished flight data from recent rotorcraft icing tests behind the HISS (U.S. Army helicopter icing spray system) tanker and at the Ottawa spray rig, it was evident that, when ice accretions exceeded approximately 1 cm on the rotor, torque rose greatly.

RESULTS AND DISCUSSION

As was noted in the previous section the pneumatic boot configurations that had a single spanwise tube at the leading edge proved to be inadequate for these deicing tests of a stationary rotor blade. Inflation of the boots at various conditions of tunnel speed, temperature, and model angle of attack resulted in the ice being severely fractured, but the ice cap would not leave either the upper or lower surfaces. After each of these tests the ice adhesion was found to be so significantly reduced that the ice could be easily removed by wiping the surface of the model. However, the aerodynamic forces would not remove the ice. Similar results were observed with both tube sizes. It was decided therefore to change the basic boot design by splitting the single spanwise tube on the leading edge into two tubes (fig. 5). With this new design the aerodynamic forces were effective in removing the ice on the suction surface. Therefore this new boot configuration was used throughout the remainder of the testing with the wake-survey probe. It must be noted, however, that these initial tests, since there was no blade rotation with the corresponding centrifugal acceleration and blade vibration, can be considered as preliminary and probably conservative. It is possible that even the single-spanwise-tube configuration would work in a real rotor environment.

Airfoil Drag

The model section drag coefficient data without ice are presented in figure 7 as a function of section angle of attack. In this figure data are presented for the clean model without the boot and for the model with the boot, both deflated and inflated. Also shown in figure 7 are published data (ref. 4) for a NACA 0012 airfoil section, both smooth and with standard roughness. These data provide a means to evaluate and validate the measurements made with the wake-survey probe. Figure 7 also includes the results of the flow separation studies, made by observing tufts, which show the effect of the pneumatic boot on the airfoil stall characteristics.

The data in figure 7 are for a tunnel speed of 67 m/sec (150 mph). As noted in the previous section, data were obtained at two tunnel speeds, 67 and 112 m/sec (150 and 250 mph). Since both speeds were well below the region where compressible flow effects become important (i.e., $M_0 \geq 0.4$), the drag coefficients were essentially the same for the two test speeds. Figure 7 shows that the clean-model data agreed very well with the smooth-airfoil reference data, thereby validating the probe results. The data with the boot installed, but uninflated, indicate a drag penalty that decreased with angle of attack. This penalty was about 20 percent at low angles and decreased to zero at higher angles. However, this penalty could probably be reduced to zero if the boot were recessed flush with the surface of the wing. In any case the penalties were less than the difference between the smooth and standard-roughness reference airfoil drag data.

The drag associated with the inflation of the boot was quite large, with drag increases ranging from about 50 percent at the low angles of attack to nearly 300 percent at higher angles of attack. Similar results were observed in the stall angle data. With the boot deflated, the stall angle of attack was about 16°, nearly the same as that of the smooth reference airfoil. When the boot was inflated, however, the stall angle was reduced to about 9.4°. This result, although severe, may still be acceptable since the rotor blade cyclic pitch excursions result in angles of attack that are typically less than 8°. Consequently accidental boot inflation should not cause blade stall.

Figure 8 presents plots of drag coefficient as a function of angle of attack for two cases: (1) data repeated from figure 7 for the inflated boot without any ice present; and (2) the envelope of the drag data taken when the test section had about 1 cm of ice on its leading edge. (Data from both rime and glaze ice conditions are included within this envelope.) As noted earlier, helicopter pilots and test engineers have told us in informal conversations that helicopters like the UH-1H can tolerate about 1 cm of ice on the main rotors without severe consequences, such as inordinate torque rise caused by ice drag or excessive shaking and vibration due to unsymmetrical ice shedding on the main rotors.

Figure 8 shows that with 1 cm of ice on the leading edge the flow separates when the angle of attack exceeds about 6°. Therefore we should expect that with 1 cm of ice the airfoil performance will deteriorate drastically for angles of attack greater than 6°. On the other hand, figure 8 shows that with the boot inflated and no ice, the airflow separated at about 9.5° and the drag coefficient was about the same or lower than it was with 1 cm of ice. We therefore conclude that, since the helicopter can fly with 1 cm of ice, the inflation of the boot with no ice should not produce severe or catastrophic results.

Deicing Performance

The pneumatic boot deicing performance and characteristics are evaluated in figures 9 to 19. In figures 9 to 13, comparing the drag measured before and after actuating the boot yields a direct indication of the boot deicing perfor-

mance. Figures 14 to 19 are a series of photographs of the boot for several deicing sequences. Figures 9 to 13 show data for the two types of icing-deicing sequences. In figures 9 and 10 the model was iced and deiced at the same angle of attack. In figures 11 to 13 the model was iced at one angle and deiced at another. In each case the first angle listed is the angle at which the model was iced, and the second is the deicing angle. Data are presented for two tunnel temperatures, namely -6.1° C (21° F) and -14.4° C (6° F). These temperatures gave representative glaze and rime ice conditions, respectively. For each temperature shown, ice accretion resulted in a significant increase in drag coefficient. However, the increases in drag coefficient were generally less at the colder temperature than at the warmer temperature. This result is consistent with the fact that rime ice shapes are smoother than glaze ice shapes. As shown in figures 9 to 13 activating the pneumatic boot at either temperature resulted in a significant decrease in these penalties. The residual drag was due to the residual ice left on the model (both on the boot and behind the boot). In each case shown, the data represent one cycle of boot inflation; however, additional cycling of the boot seemed to have little additional effect on removing the residual ice. The residual drags shown are therefore a direct measurement of the boot performance, and as shown in figure 9 the boot was quite effective especially at the warmer temperatures. The boot tended to be less effective at the colder temperatures, but in each case the boot resulted in a reduction in drag that could be the difference between a rotorcraft completing its mission or getting into serious difficulty. For example, in figure 13 (for T_0 = -14.4° C) even though the residual drag at the cold temperatures was 55 percent, activating the boot at 9.4° angle of attack resulted in the flow over the blade reverting from a separated to an attached condition. Comparing the two types of icing-deicing sequences tested did not show any definite trend. It is inconclusive whether the slow variation in cyclic pitch used here could in any way be representative of the real rotor motion.

Typical icing-deicing sequences are depicted in figures 14 to 19 for both the upper (suction side) and lower (pressure side) surfaces. Figures 14 to 17 show the glaze icing condition (i.e., at warmer temperatures) at two different angles of attack. As shown in these photographs the icing limits along the chord, since both of these test points were at positive angles of attack, were greater on the lower surface than on the upper surface. Also the icing limit on the lower surface increased with increasing angle of attack. Figures 18 and 19 show a rime ice condition. Compared with the previous two photographic sequences, the ice at this lower temperature was much whiter and grainier and was not as peaked or double-horn shaped at the leading edge. In each of the deicing cases shown, the boot was fairly effective in removing ice on the upper surface but not as effective in removing ice on the lower surface. Also the effectiveness of removing ice from the lower surface was less at the lower temperatures. Comparing these results with the drag results given previously indicated that most of the observed drag rise resulted from the ice on the upper surface. This was especially evident for the rime ice case (figs. 18 and 19), where very little of the lower ice was removed but, as shown in figure 13 (for T_0 = -14.4° C), the drag was reduced from a large value with separated flow to a lower value with attached flow. Again, as shown in figures 14 to 19, the residual ice was greater for the rime ice case and resulted in higher residual drags. In all the sequences shown the residual ice was well fractured, and

therefore the boot performance should be better if the centrifugal and vibratory forces on a real rotor were present.

NASA Ames-Lewis Rotor Program

The next step in this program is to see how pneumatic deicer boots perform on full-scale rotating blades. NASA Ames has begun a program to test boots on a UH-1H helicopter. A series of nonicing tests will first be performed - including tie-down, hover, and full-flight evaluation. If these nonicing tests are successful, icing tests should follow.

CONCLUDING REMARKS

These initial tests of a pneumatic deicer boot on a helicopter rotor blade yielded some answers to several of the basic aerodynamic questions posed by the Lockheed-California Company in 1973. Since the blade was fixed in the tunnel (nonrotating) and since the tunnel speeds were limited to Mach numbers less than 0.4, these tests could not simulate the mechanical, rotational, cyclic pitch, vibrational, and high-tip-speed environment of an operational rotor. However, some important results were observed. First, the drag penalties of uninflated boots were small as compared with drag penalties caused by 1 cm of ice. These penalties were no worse than experienced with today's blade foreign-object-damage shields and would probably be eliminated if the boots were recessed flush on new blade designs. Second, although the aerodynamic effect of inflating the boot without ice was sizable, for most angles of attack the penalties were no worse than those already accepted on fixed-wing aircraft. Even the relatively larger tube diameters on the small-chord airfoil did not lower the stall angle into the normal region of rotor operation. At the same time these penalties proved to be significantly less than those observed with 1-cm accretions of ice. Third, the pneumatic boot proved to be an effective deicer even at low temperatures (-14.4° C) and in a probably very conservative test environment. It must be noted, however, that some of these results could be different on a real rotor, especially the aerodynamic effects at the higher tip speeds, but in that case the deicing performance would probably be more effective.

Because the pneumatic boot effectively reduced the icing drag penalty without causing any other serious aerodynamic penalties, NASA Ames has begun a program that includes full-scale flight testing of the pneumatic boot on helicopter rotors. If the boot material withstands the severe rotor environment in flight and if no further significant aerodynamic penalties arise, perhaps the pneumatic boot can be developed into a lightweight, low-cost, low-power, and easily maintained deicer system for rotor applications.

REFERENCES

1. Aircraft Icing. NASA CP-2086, 1979. (Also FAA-RD-78-109.)

2. Werner, J. B.: Ice Protection Investigation for Advanced Rotary-Wing Aircraft. LR-25327-10, Lockheed-California Co., 1973. (USAAMRDL-TR-73-38, AD-771182.)

3. Bowden, Dean T.: Effect of Pneumatic Deicers and Ice Formations on Aerodynamic Characteristics of an Airfoil. NACA TN-3564, 1956.

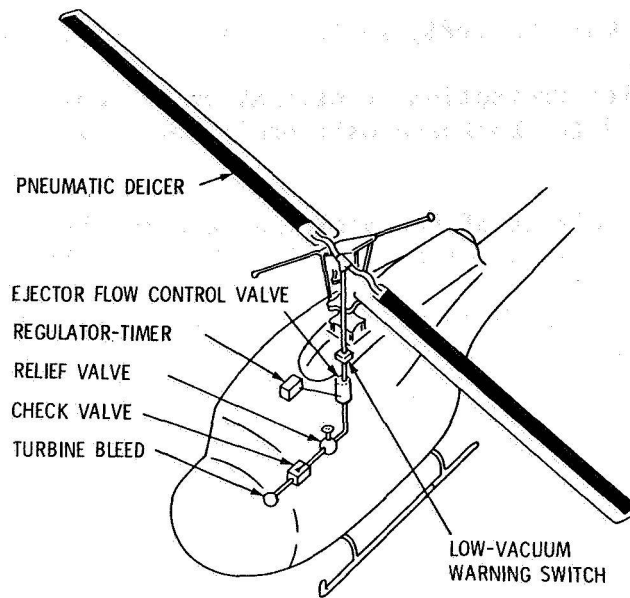4. Abbott, Ira H.; and von Doenhoff, Albert E.: Theory of Wing Sections. Dover Publications, Inc., 1959.

PNEUMATIC DEICER

EJECTOR FLOW CONTROL VALVE
REGULATOR-TIMER
RELIEF VALVE
CHECK VALVE
TURBINE BLEED

LOW-VACUUM
WARNING SWITCH

Figure 1.- Main rotor application pneumatic deicer.

Figure 2.- Pneumatic boot on rotor model
installed in 6 × 9 ft. NASA Lewis Icing
Research Tunnel.

434
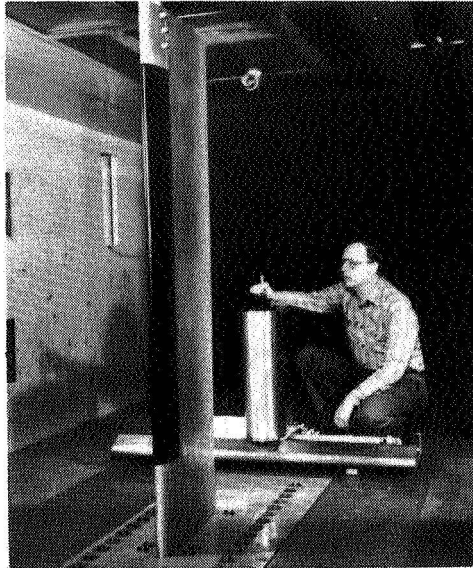
Figure 3.- Pneumatic boot on rotor model and wake
survey probe in NASA Lewis Icing Research
Tunnel.

$$\text{MODULE FUNCTION: } \frac{V}{V_0} = \left(\frac{H - p_0}{H_0 - p_0} \right)^{1/2}$$
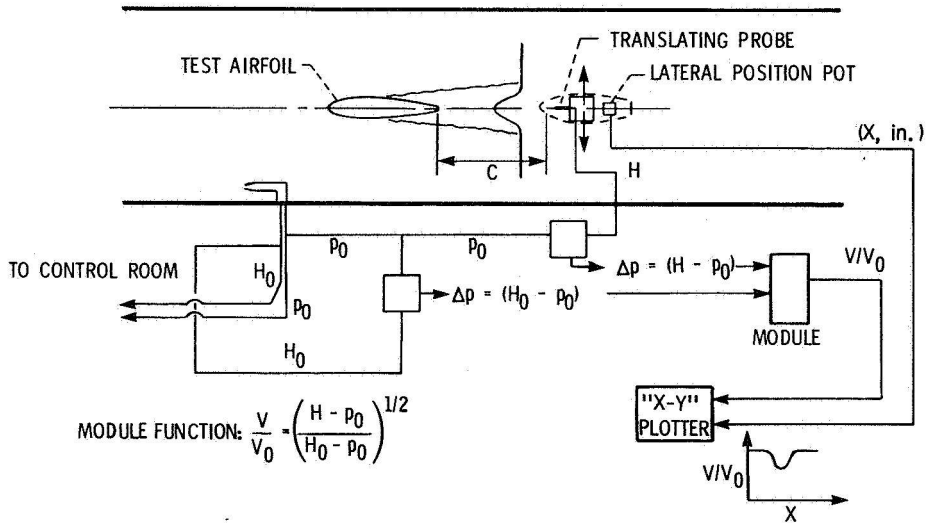
Figure 4.- Translating probe instrumentation.
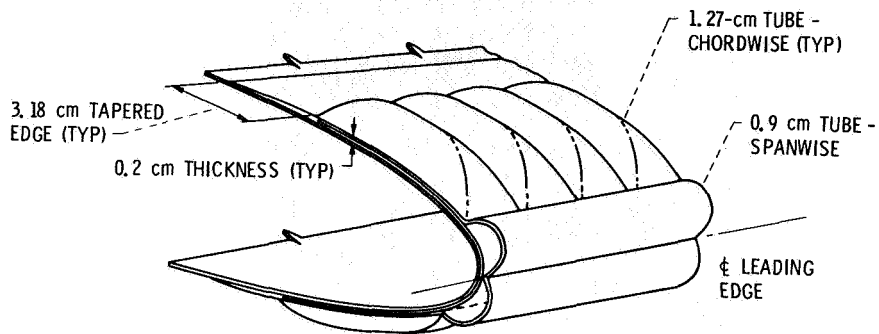
Figure 5.- Typical cross section of installed deicer (inflated), small tube.
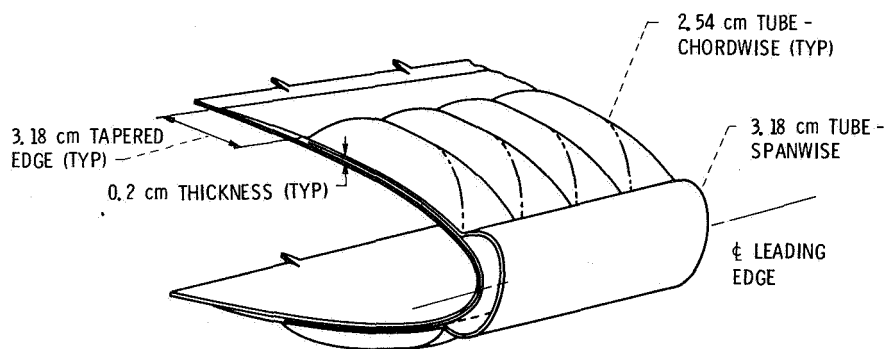
Figure 6.- Typical cross section of installed deicer (inflated), large tube.

436
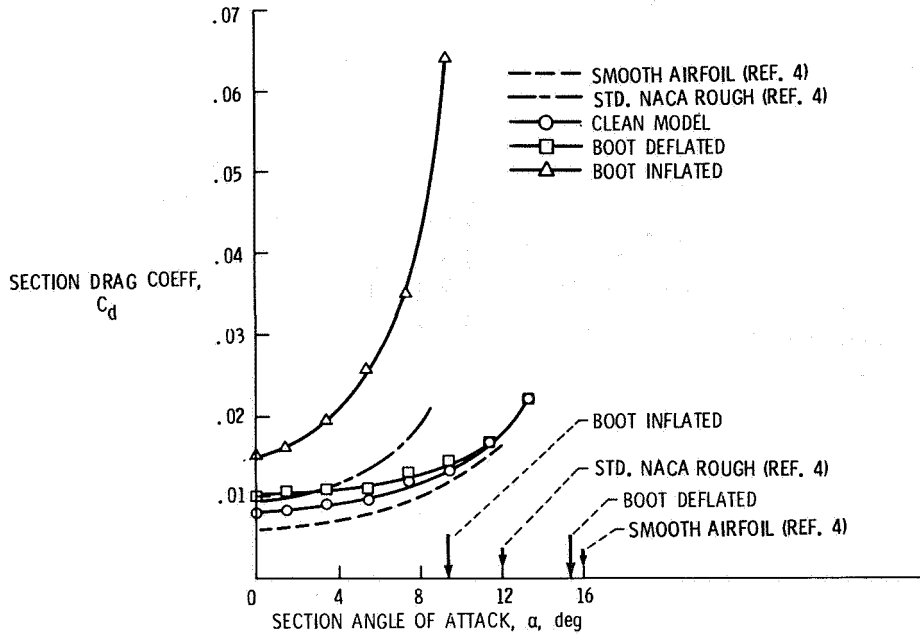
Figure 7.- Helicopter rotor model section drag.
NACA 0012 airfoil (no ice); V = 67 m/sec.
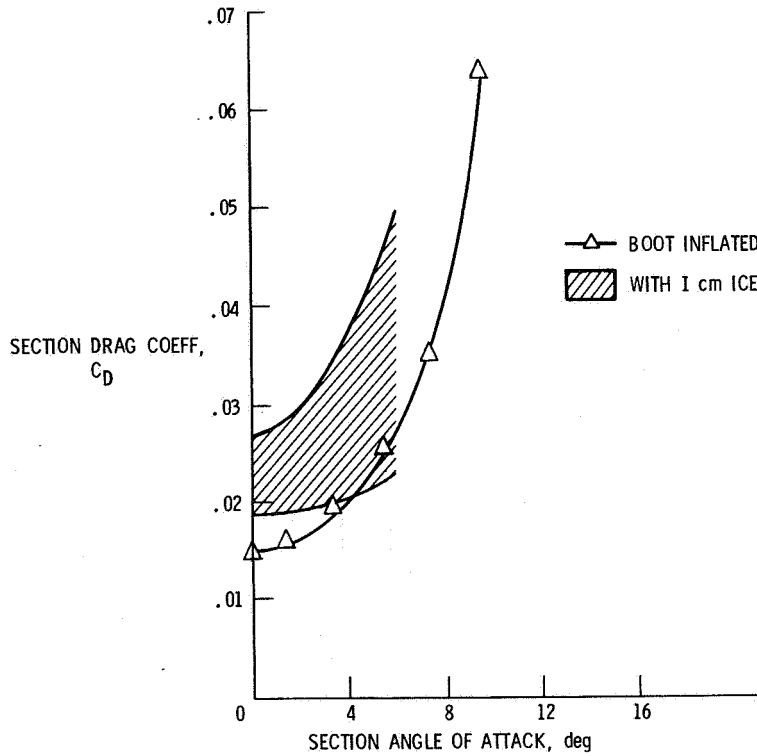
Figure 8.- Helicopter rotor model section drag.
NACA 0012 airfoil; V_0 = 112 m/sec.
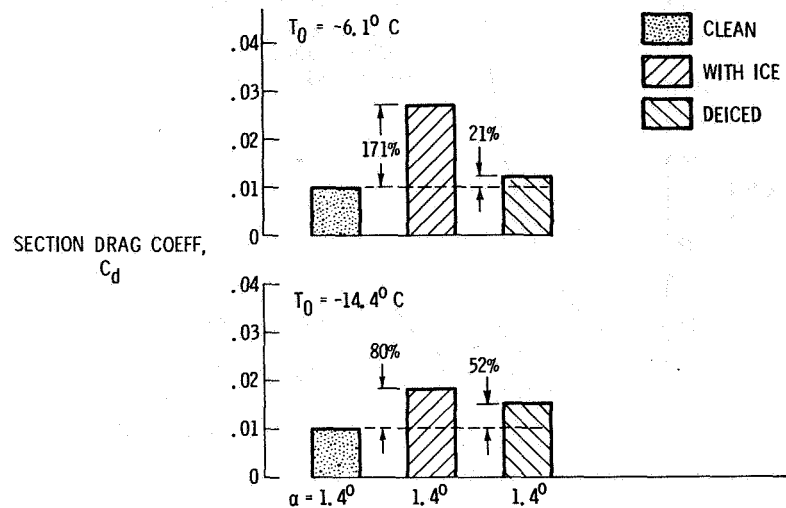
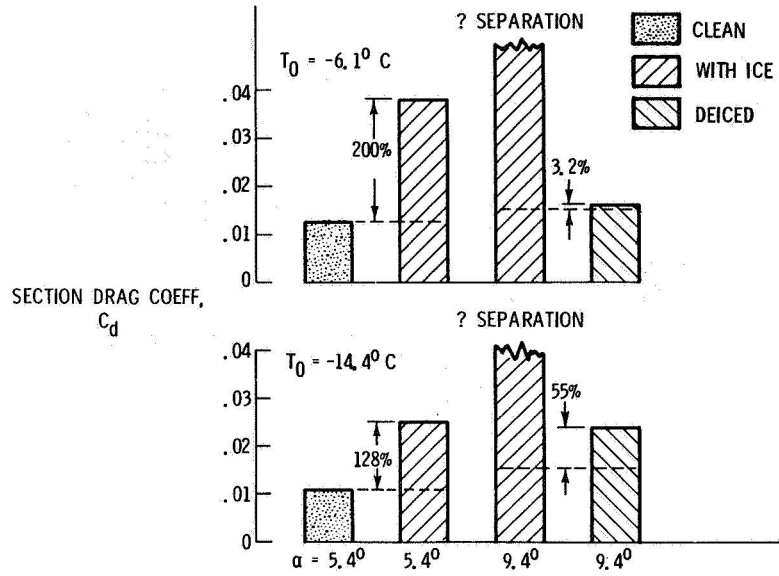Figure 9.- Section drag of helicopter rotor model with pneumatic boot. Ice-deice sequence; $\alpha = 1.4°/1.4°$; $V_0 = 112$ m/sec.
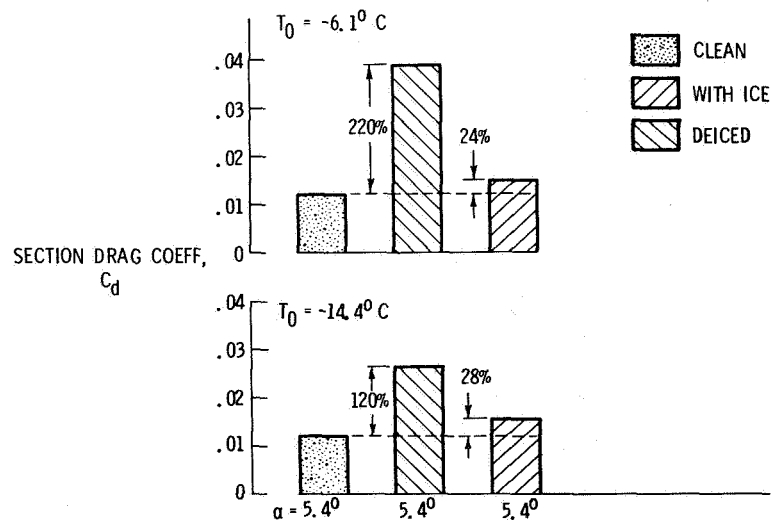
Figure 10.- Section drag of helicopter rotor model with pneumatic boot. Ice-deice sequence; $\alpha = 5.4°/5.4°$; $V_0 = 112$ m/sec.
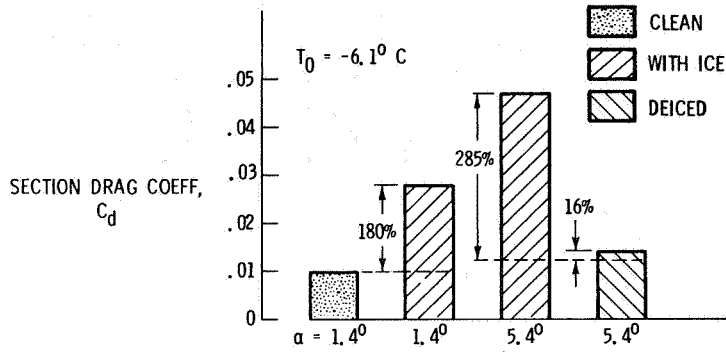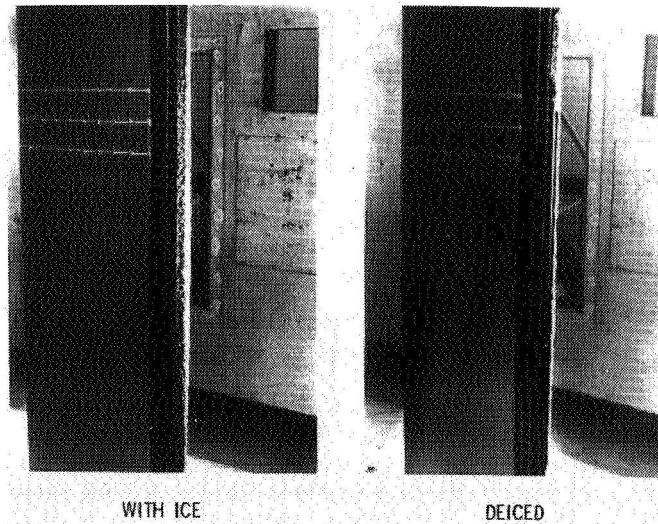
Figure 11.- Section drag of helicopter rotor model with pneumatic boot. Ice-deice sequence; $\alpha = 1.4^{\circ}/5.4^{\circ}$; $V_0 = 112$ m/sec.
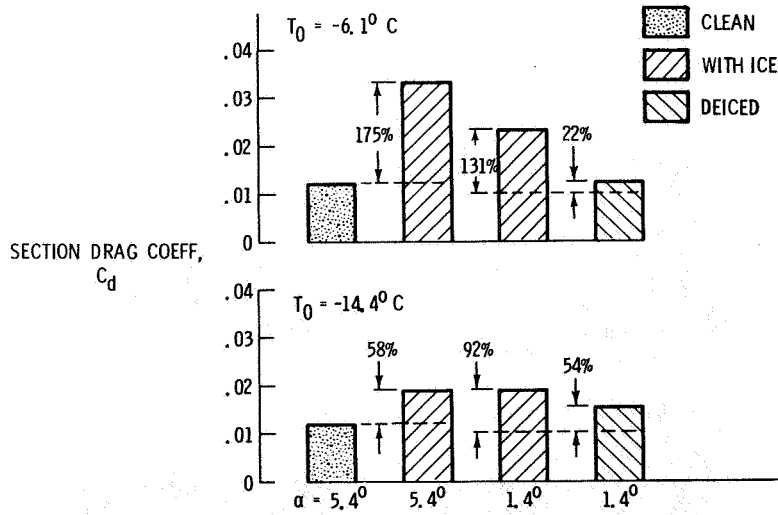
Figure 12.- Section drag of helicopter rotor model with pneumatic boot. Ice-deice sequence; $\alpha = 5.4^{\circ}/1.4^{\circ}$; $V_0 = 112$ m/sec.

Figure 13.- Section drag of helicopter rotor model with
pneumatic boot. Ice-deice sequence; $\alpha = 5.4°/9.4°$;
$V_0 = 112$ m/sec.

Figure 14.- Typical ice-deice sequence. Upper surface;
$\alpha = 1.4°/5.4°$; $T_0 = -6.1°C$; $V_0 = 112$ m/sec.
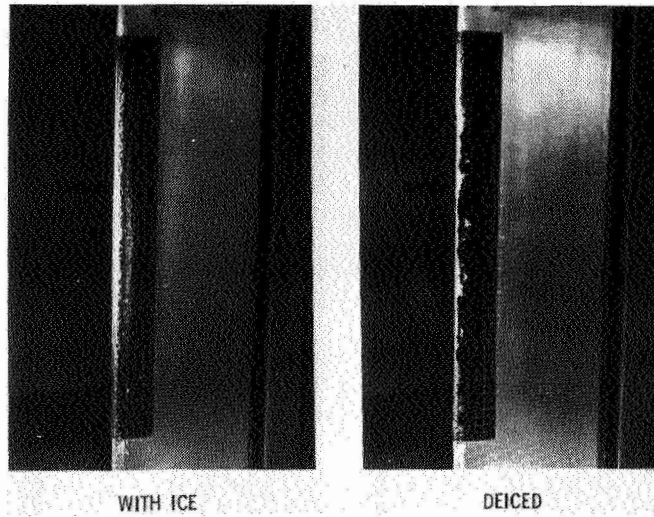
Figure 15.- Typical ice-deice sequence. Lower surface;
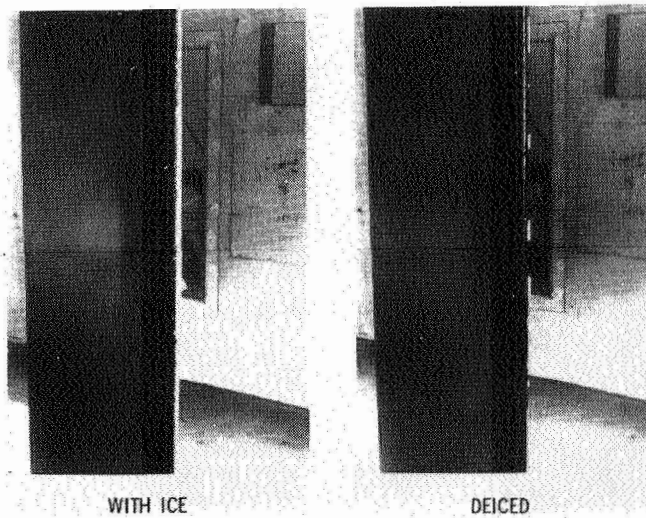$\alpha = 1.4^{\circ}/5.4^{\circ}$; $T_0 = -6.1^{\circ}C$; $V_0 = 112$ m/sec.

Figure 16.- Typical ice-deice sequence. Upper surface;
$\alpha = 5.4^{\circ}/5.4^{\circ}$; $T_0 = -6.1^{\circ}C$; $V_0 = 112$ m/sec.

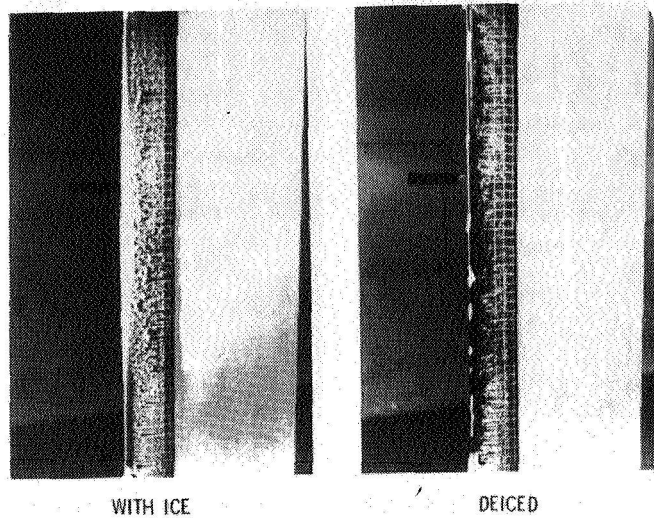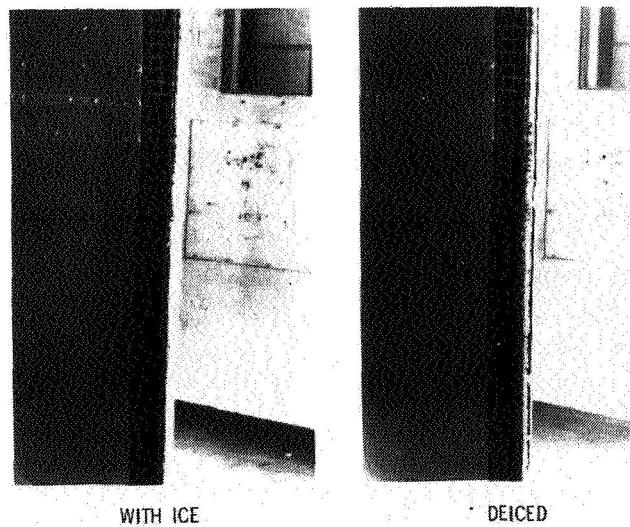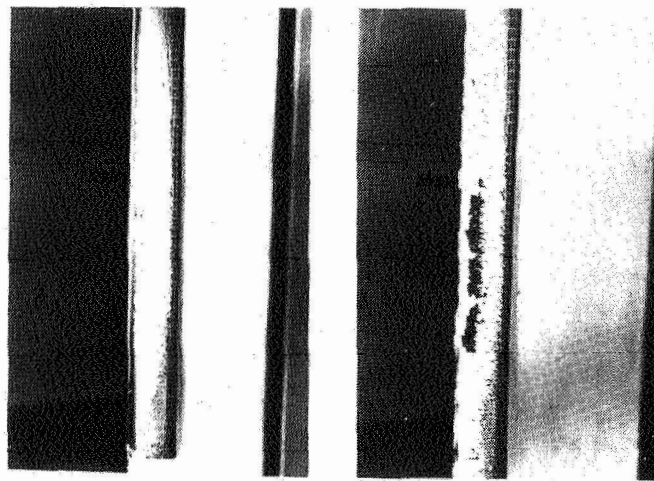WITH ICE   DEICED

Figure 17.- Typical ice-deice sequence. Lower surface;
$\alpha = 5.4^o/5.4^o$; $T_0 = -6.1^oC$; $V_0 = 112$ m/sec.

WITH ICE   DEICED

Figure 18.- Typical ice-deice sequence. Upper surface;
$\alpha = 5.4^o/9.4^o$; $T_0 = -14.4^oC$; $V_0 = 112$ m/sec.

442

WITH ICE   DEICED

Figure 19.- Typical ice-deice sequence. Lower surface;
$\alpha = 5.4^{\circ}/9.4^{\circ}$; $T_0 = -14.4^{\circ}C$; $V_0 = 112$ m/sec.